ISSN 0038-0946, Solar System Research, 2009, Vol. 43, No. 2, pp. 143–150. © Pleiades Publishing, Inc., 2009.
Original Russian Text © S.A. Bogachev, V.V. Grechnev, S.V. Kuzin, V.A. Slemzin, O.I. Bugaenko, I.M. Chertok, 2009, published in Astronomicheskii Vestnik, 2009, Vol. 43, No. 2, pp. 152–159.

On the Processing and Analysis of the Data of the CORONAS-F/SPIRIT and Other Solar Experiments

S. A. Bogachev[a], V. V. Grechnev[b], S. V. Kuzin[a], V. A. Slemzin[a], O. I. Bugaenko[c], and I. M. Chertok[c]

[a] *Lebedev Physical Institute, Russian Academy of Sciences, Leninskii pr. 53, Moscow, 117924 Russia*
[b] *Institute of Solar-Terrestrial Physics, Siberian Branch of the Russian Academy of Sciences, ul. Lermontova 126, Irkutsk, 664033 Russia*
[c] *Sternberg Astronomical Institute, Moscow State University, Vorob'evy gory, Moscow, 119992, Russia*

Received February 27, 2008

Abstract—More than 300000 solar images in the extreme ultraviolet and soft X-ray regions were obtained using two telescopes and four spectroheliometers of the CORONAS-F/SPIRIT device from August 2001 to December 2005. Methods for the processing of such data and extracting physical information are presented, taking into account the experience of processing and analysis of other space experiments on solar research. Some results on applications of the considered methods are presented.

PACS: 95.40.+s; 95.55.Aq; 95.75.Mn; 95.85.Mt,Nv

DOI: 10.1134/S0038094609020075

INTRODUCTION

Primary solar images arriving at the Earth from spacecrafts often contain instrumental artifacts superimposed on the desired signal, distort it, and complicate its processing and analysis. Instrumental effects can be interpreted as erroneous physical phenomena. The ground-based groups providing experiment performance usually carry out preprocessing of such images. At the same time, they themselves correct some artifact types which are simple in processing and have no significant effect on a further analysis of the data; for other artifacts, the software is presented to a researcher, which he can use by himself.

When operating with instrumental data, it is important to understand that any influence on them is accompanied by data loss or distortion. From this point of view, it would be better to put a software package at researchers' disposal which provides data processing and analysis, rather than transformed files. In this case, a researcher gets the opportunity to decide by himself which changes are acceptable for solving a problem facing him and which are unacceptable, hence, to choose processing versions. However, the experience of SPIRIT data processing showed that it is reasonable to correct some image features immediately, since they seriously complicate the further use of the data. In this study, by the example of SPIRIT images, we consider instrumental and other features on telescopic images of the extreme ultraviolet region and describe the methods used for their elimination. We also review some methods used in the scientific analysis of images.

FEATURES OF IMAGES OBTAINED BY SPACE TELESCOPES

Let us list the main factors which lead to loss or distortion of data arriving at the Earth from spacecrafts. Significant difficulties in image processing arise due to the background summed with the desired signal. As a rule, a radiation receiver of modern telescopes is the CCD array; at its output, a noise signal always exists even in the absence of incident light. Moreover, scattered radiation significantly contributes to the background. On average, the background level on the SPIRIT images typically does not exceed 5% of the average signal, although this ratio can increase in some image areas.

The second factor is lost data. The data from the array arrives at the input of the data collection and recording system of a spacecraft and is then transmitted to the Earth by digital packets, a part of which can be lost or distorted during a communication session. During imaging, empty regions appear in the place of such lost packets, whose shape and size depend on the telemetric file format. For example, on the SOHO/EIT images, the lost packets are shaped as 32×32 pixel squares; on the SPIRIT images, they are the lines whose length is controlled by the compression ratio of the telemetric data.

The third factor affecting the quality of satellite images is nonlinear and spatially nonuniform attenuation of radiation during its passage through telescope systems. The combined effect of all these factors is sometimes united by the term "flat field function." For example, the optical systems of SPIRIT telescopes

incorporate filters transmitting only radiation of an operating range to the photodetector. Filter damages during orbital operation caused an attenuation of the transmitting radiation, which was taken into account in the white field function. In addition to filters, image converters and photodetectors can significantly contribute to the flat field function, since their sensitivity is usually nonuniform over the image field.

The fourth distorting factor is sometimes called the "snow" or "snow storm." In powerful proton events, a significant number of energetic particles are produced, which propagate from the Sun to interplanetary space. After a certain time, these particles reach a spacecraft and appear on images as bright dots or bands resembling snow. The "snow" on images also appears when a spacecraft enters the Earth's radiation belts and polar cap regions. During processing of the solar images obtained by the SPIRIT, it was required to additionally solve the image centering problem. The solar disk center on images shifts with time due to the satellite axis motion, thermal deformations, and other factors whose combined effect is unpredictable. At the same time, to analyze physical processes in the heliosphere, it is often necessary to involve data of several spectral ranges obtained using various telescopes. Certainly, in this case, image alignment accuracy should be no worse than the spatial resolution of telescopes. Since the orientation system of the CORONAS-F satellite (onboard which the TESIS experiment was performed) did not yield data on the current position of the satellite platform, the problem of SPIRIT image centering was solved using special mathematical methods.

LOST DATA RECOVERY AND FLAT FIELD CORRECTION

The capability of lost data recovery for the SPIRIT telescopes is better than that of similar EIT telescopes onboard the Solar and Heliospheric Observatory (SOHO) satellites due to the line-by-line transmission of data packets (it is block-by-block at the EIT). Since the pixel size of the SPIRIT telescope images was smaller than their spatial resolution, it made it possible to recover lost lines with a minimum of introduced distortions.

To recover lost data on images, in principle, two methods can be used. One is used when there exists an image closely spaced in time with an image obtained in the same channel. In this case, the data lost in the first image can be copied from the second one. However, in practice, this method rarely yields satisfactory results, since even images closely spaced in time differ by background levels, exposures, and other factors. Moreover, direct copying of data from one image to another requires their alignment with an accuracy exceeding the pixel size, which is almost unachievable. As the SPIRIT experience has shown, better results are achieved when filling lost data by values obtained by interpolation of data from adjacent lines. In practice, a good result was obtained using the interpolation between four adjacent points, given by the formula

$$X_i = X_{i+1} + X_{i-1} - \frac{1}{2}(X_{i+2} + X_{i-2}).$$

During the recovery of the flat field function, it should be taken into account that such a function is common for all images of one channel. This means that a single field matrix can be constructed for each channel. We call the matrix field a table of numbers whose size is identical to that of the CCD array, and the values are equal to unity for those pixels where radiation is transmitted through the filter without distortions and exceed unity in those pixels where radiation is absorbed in the filter. As a result, to restore an image, it is sufficient to multiply the data matrix read from the CCD array by the field matrix of a given channel. We do not describe the methods for calculating the flat field, since they are described in detail in published data. As for the SPIRIT telescopic channels, a method presented by Kuhn et al. (1991) was applied to them.

BACKGROUND SUBTRACTION AND IMAGE CENTERING

For background subtraction and image centering, the SPIRIT team has developed special software available for external users. The background on SPIRIT satellite images (as for most space telescopes) is nonuniform over the frame field and cannot be removed by simple subtraction of a constant baseline. Moreover, the background distribution varies from frame to frame, i.e., the matrix should be calculated individually for each image, in contrast to the flat field matrix common for all images of one channel.

To subtract the background in SPIRIT images, the following method was developed which showed high efficiency for the EIT data as well. For each SPIRIT channel, a set of several tens of shadow frames (images obtained with a closed shutter) was composed. These frames can be interpreted as two-dimensional background matrices F_i differing by their spatial distribution and brightness. We further assume that the background of any image can be presented as the sum of functions F_i with certain coefficients,

$$Back = a_0 + \sum a_i F_i. \quad (1)$$

Thus, the problem of constructing the background matrix is reduced to the problem of determining the set of coefficients a_i individual for each image. To this end, a set of values was read from an image at several thousands of points beyond the solar disk. Then, the coefficients a_i were selected as to minimize the sum of squared deviations between values at the image points and the same points in the background matrix (1). The resulting data of the use of the method are shown in Fig. 1.

We also have developed software for coordinate determining and telescopic image centering. The corre-

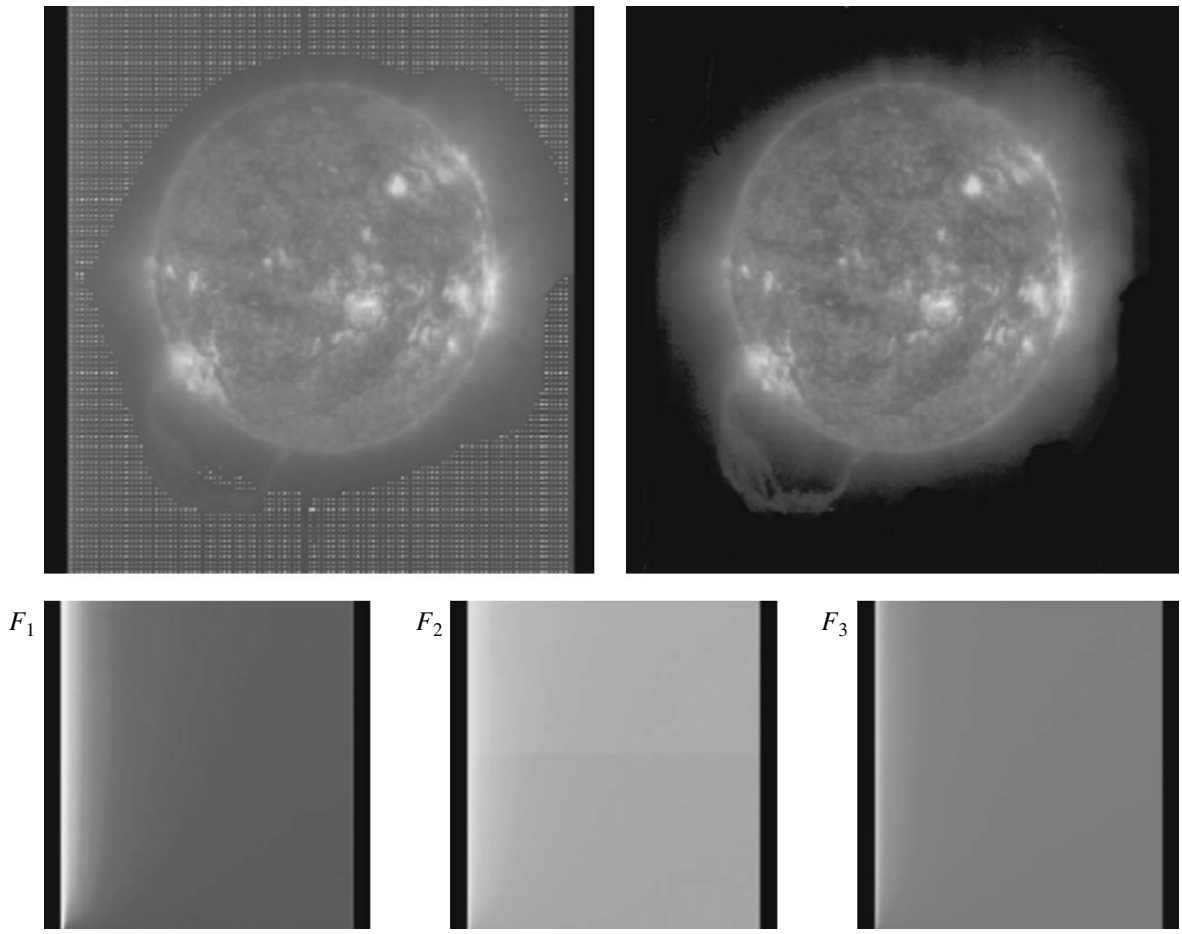

Fig. 1. Background subtraction from the solar image. The top panel shows the image before background subtraction (the points used to determine the coefficients a_i are shown) and after subtraction. The bottom panel shows the examples of dark frames used as basis function F_i.

sponding technique is based on finding the solar limb on the image under study. The limb was searched by successive iterations during line-by-line scanning of the image. The determination of the limb point depends on the channel in which the image was obtained. In 175 Å and 195 Å channels, where basic radiation is produced by coronal plasma, the limb is determined by the maximum image brightness; in the He II 304 Å channel, in which plasma radiation of the transition layer is mainly recorded, the limb is determined by the maximum brightness gradient corresponding to the solar disk transition to "sky." The range in which limb points are searched at each iteration step depends on the scatter (dispersion) of the points found at the previous iteration. As a rule, the method converges after three to four iterations. The accuracy of the determination of the solar disk center is half the pixel size (for SPIRIT images, it is ~2″). This method is illustrated in Fig. 2.

METHODS OF SECONDARY PROCESSING AND ANALYSIS OF IMAGES

After image centering, background subtraction, flat field correction, and suppression of other instrumental features, a researcher is faced with the problem of physical information extraction from images. We call the methods used at this stage the secondary processing methods, in contrast to the primary processing methods directed to improve the image quality and reduce images to standard scales, orientation, and formats (see Grechnev et al., 1999; Grechnev, 2002).

Scientific information contained in solar images is extraordinarily diverse. Hence, the methods for its extraction and analysis are also very diverse (see, e.g., Bugaenko, et al., 2004). Here we describe only some of them associated with the analysis of a large series of sequential images. Such data are widely used, while methods of their processing are not as developed and

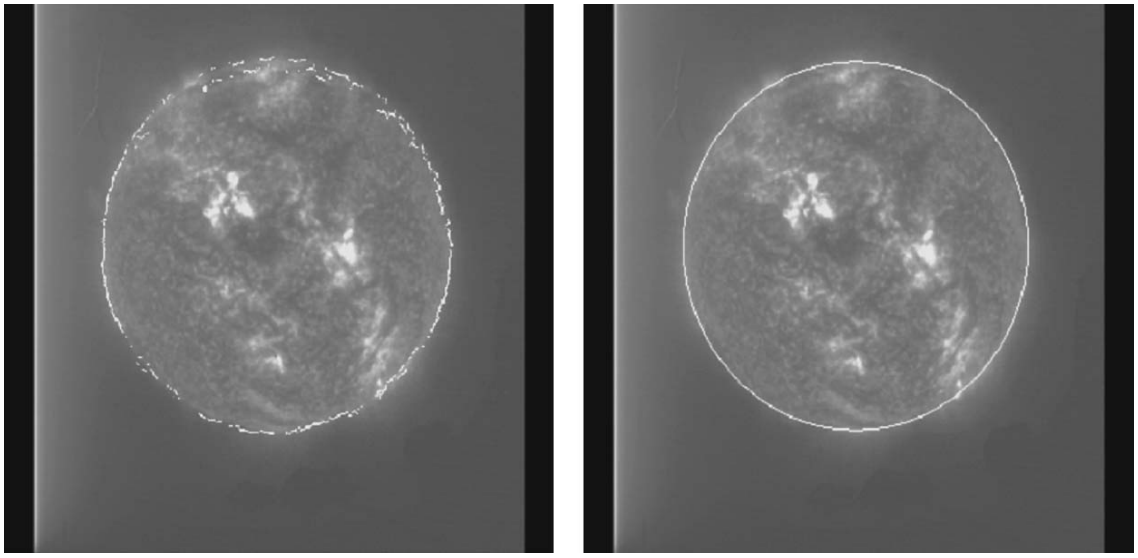

Fig. 2. Determination of the limb position on the SPIRIT image. The left panel shows the initial image with the limb points determined by the first iteration cycle. The right panel shows the result of the third final iteration cycle.

available as methods for the processing and analysis of individual images.

The processing of image series has two important features. First, a good alignment of series frames is required so that possible "jitter" would not complicate image comparison. Such jitter can be eliminated, e.g., by the method based on the calculation of correlation coefficients between images and the selection of such a position that the correlation between adjacent frames would be maximum. The second feature is that all series images should be reduced to identical brightness characteristics (Slemzin et al., 2005). Such a photometric calibration is especially important during the quantitative analysis of data.

Nonlinear Representation of Images

Soft X-ray and EUV images are characterized by a very high dynamic range due to a wide range of emission values of observed coronal structures. In some cases, it can be contracted by limiting brightness levels from above and from below. Noises such as white or black dots in some images can significantly lower the contrast if these local defects have very high and low values. In this case, median smoothing can significantly improve the contrast. However, in this case, the spatial resolution becomes poor. Another powerful but very rough method is leveling the brightness distribution histogram. This nonlinear transformation makes the brightness distribution uniform over the image. The essence of the method consists in removing the values with low statistical significance or which are entirely absent in the image. The dynamic range in the images processed by this method is sharply contracted. As a result, the contrast significantly decreases and both very bright and very weak details become simultaneously visible, which facilitates the detection of low-contrast details on the image. This method is universal and makes it possible to see the general picture of coronal structures on any soft X-ray EUV image (SOHO/EIT, Transition Region And Coronal Explorer (TRACE), Yohkoh/SXT, CORONAS-F/SPIRIT satellites). The softest method of image representation is the use of logarithmic or power-law scaling of sets.

Difference Methods

Difference methods are used to study low-contrast phenomena and the structures whose brightness is small in comparison with surrounding structures. In this case, two images are taken, one is subtracted from another, and the difference pattern is used to determine what and where changes occurred for the time between these two frames.

One of the difference methods widely used, in particular, to detect coronal mass ejections (CME) and coronal waves is that of an image immediately preceding each frame being subtracted from the latter. This method is called the running difference. During its application, it is important to understand that the difference images obtained by this method show the time derivative of the brightness distribution, rather than the distribution itself, and artifacts existing on the images are also differentiated.

In the second difference methods, the same image obtained before an event onset is subtracted from all frames. However, in this case, artifacts can arise on images due to solar rotation (this effect is most pro-

nounced for structures arranged along the meridian). To avoid this effect, the solar rotation is compensated on all images by transforming the spherical coordinates before subtracting the frames.

The method of difference frames with a fixed baseline and preliminary compensation for solar rotation is very efficient to study the dimming, i.e., a temporary decrease in the coronal structure brightness occurring during many CME. This method is used to analyze the SOHO/EIT data (Chertok, Grechnev, 2003a; 2003b; 2005); currently, it is efficiently applied to analyze the CORONAS-F/SPIRIT data (Chertok et al., 2004; Grechnev et al., 2005; Slemzin et al., 2004; 2005; Kuzin et al., 2006). We note that dimmings are relatively weak phenomena: the decrease in the brightness of them usually does not exceed a few percent of the maximum image brightness. Therefore, it is necessary to limit the image brightness range in studying them by difference methods.

In Fig. 3, the two described difference methods are illustrated by the example of the SOHO/EIT data in the 195 Å channel for the event of October 28, 2003. The left column (A) presents the initial images with leveled histograms. Column B shows the difference images obtained by the running difference method. The images in column C were obtained by the method with a fixed baseline of 10:48 UT, but disregarding solar rotations. This rotation was taken into account in column D.

Dimmings are quantitative studied by analyzing and comparing brightness variations in small areas (see, e.g., Zarro et al., 1999; Slemzin et al., 2005). The time profiles constructed by this method allow us to estimate the darkening depth and to compare the phenomenon evolution in various solar disk areas.

Suppression of Particle Tracks in Images

The efficient procedure of "snow" suppression is incorporated in the SOHO software. In this procedure, "snowflakes" (particle tracks) are detected by a brightness excess over the brightness in an image subjected to median smoothing with a window width of 7. Pixels within "snowflakes" are replaced by pixels of the smoothed image. The suppression efficiency of particle tracks can be increased by involving adjacent frames. Moreover, there are additional possibilities of increasing the dimming study efficiency when only coronal structure darkenings are important and there is no need to detect brightenings. We have developed methods which take into account these circumstances (Grechnev, 2004; Chertok, Grechnev, 2005). One of them consists of forming difference images which show only darkenings. This is especially useful when only two images are available—one before and another after an event. In this case, a minimum value of this pixel in both images is assigned to each pixel of the image from which the base frame is subtracted and the corresponding pixel of the difference image x_{ij}^{dif} is formed as $x_{ij}^{\mathrm{dif}} = \min\{x_{ij}^0, x_{ij}^1\} - x_{ij}^0$, where subscripts 0 and 1 correspond to the images before and after an event. Thus, the difference image pixels are either zeros if the brightness did not decrease or are negative if the brightness decreased.

An even simpler method consists in the formation of difference images in which each pixel of the subtracted image is replaced by a minimum of adjacent ones,

$$x_{ij}^N = \min\{x_{ij}^{N-k} \ldots x_{ij}^{N+k-1}\},$$

where N is the frame number and $2k$ is the "filtering window" width (the number of images used to suppress particle tracks). It is clear that artifacts in such an image are restricted to the value of $2k$ and brightenings within the window width will be appreciably suppressed.

The complete image restoration is performed by a more complex method. In this case, we find snow "flakes" on images as pronounced isolated brightenings with respect to adjacent frames and then replace the value of each pixel within them by its minimum value in adjacent images.

Dispersion Map Method

A researcher often has to deal with large data sets, e.g., in studying solar flares, when identification of active flare sources and their dynamics requires the analysis of tens, hundreds, and even thousands of frames. To find active flare sources in these series, the dispersion map can be used. Such a map represents dynamics of an entire event in one and only one image (Grechnev, 2005). The dispersion map is obtained by calculating the dispersion in each spatial point of the data cube along its time measure. The dispersion map σ_{ij}^2 for the data cube x_{ijk} can be calculated by the formula

$$\sigma_{ij}^2 = \frac{1}{N}\sum_{k=1}^{N} x_{ijk}^2 - \frac{1}{N^2}\left(\sum_{k=1}^{N} x_{ijk}\right)^2,$$

where $i = 1, 2, \ldots, L$ is the image line number, $j = 1, 2, \ldots, M$ is the column number, and $k = 1, 2, \ldots, N$ is the number of the image "layer" in the data cube with dimension $L \times M \times N$. This expression is equivalent to the dispersion definition but does not contain cross terms. This makes it possible to avoid repeated scanning of the data cube and to decrease the calculation time. The value of each point on such a map reflects the time variability of this space point. Therefore, variable sources appear in the dispersion map: sources with variable brightness, moving, fluctuating ones, and so on, certainly according to the statistical significance of their variability.

Regular instrumental effects also appear on the dispersion map (e.g., side lobes of the instrumental function). This allows one to judge whether or not a source can be an instrumental effect. We recommend rejecting weak sources if their time profiles reproduce variations of a main flare source responsible for side lobes.

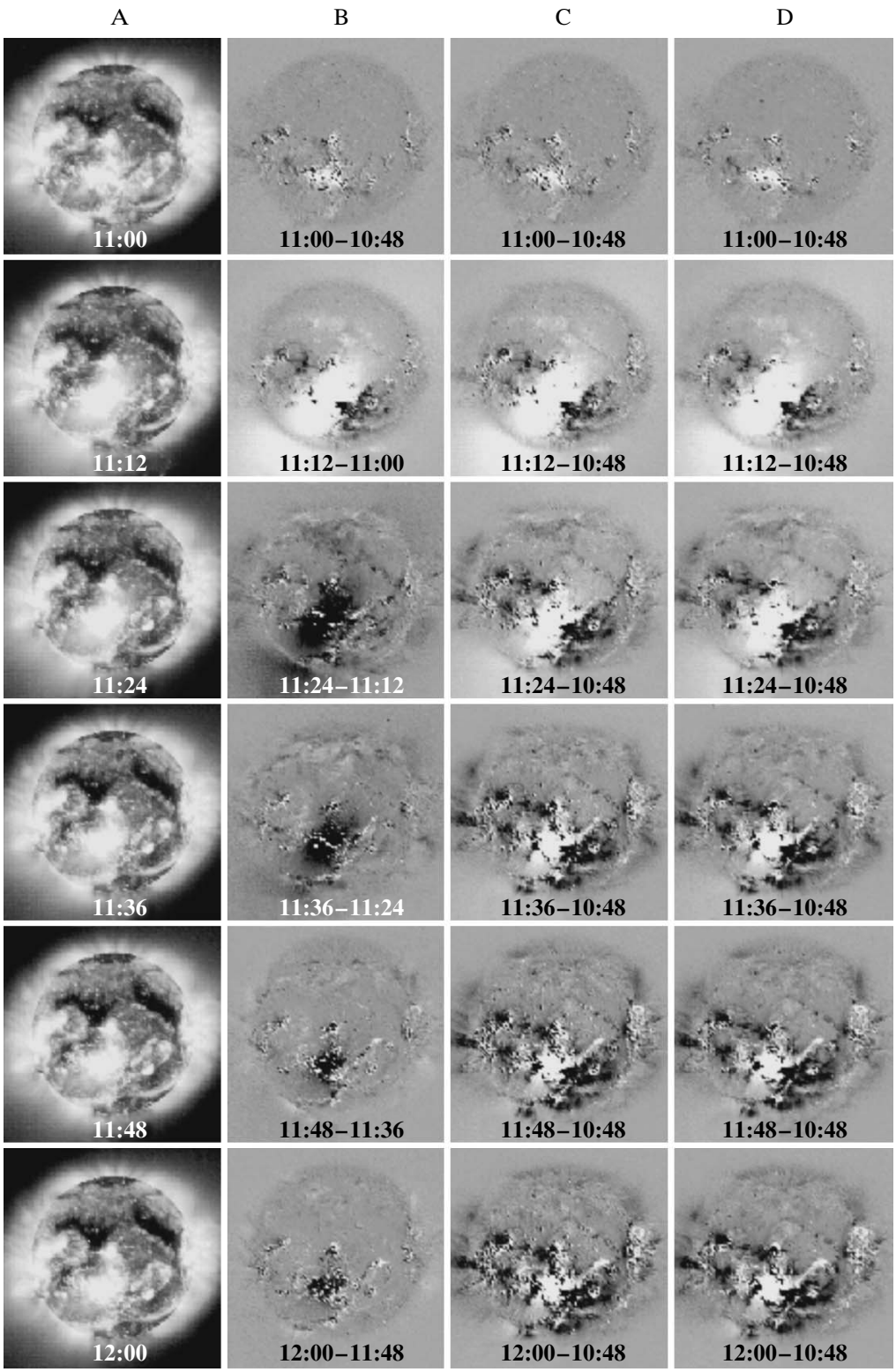

Fig. 3. Methods for obtaining difference images by the example of the SOHO/EIT data in the 195 Å channel for the event of October 28, 2003. Column A: initial EIT images. Column B: images obtained by the "running difference" method. Column C: difference images obtained by the fixed baseline method without compensation for solar rotation. Column D: the same as column C, but with preliminary compensation for solar rotation. The base frame in the bottom series was obtained five hours earlier than others.

This method was used previously to analyze sets of radio images of solar flares (Grechnev et al., 2002; Grechnev, 2003), to study quasi-periodic oscillations in active regions by optical data (Tsiropoula et al., 2000) and radio data (Nindos et al., 2002), and to study evolutions of photospheric magnetic fields (Kundu et al., 2001).

CONCLUSIONS

Using the above data analysis methods, the quality of the SPIRIT database images was significantly improved and a number of scientific results were obtained. Large-scale phenomena, in particular dimmings and coronal waves, were studied in a number of powerful eruptive events in the periods of high activity during maximum and descending phases of solar cycle 23 (see Zhitnik et al., 2005; Slemzin et al., 2005; Chertok et al., 2005; Grechnev et al., 2005). The global nature and homology of these phenomena were detected, as well as the difference in darkening times of structures in the 304 Å channel with respect to coronal emission lines, which implies a gradual downward evolution of the dimming to the transition layer (Chertok et al., 2005). It was found that the mechanisms responsible for the formation of dimmings and coronal waves are different in the general case, and the coronal wave fronts with increased brightness are probably caused by radiation of plasma with a temperature above 10 MK (Grechnev et al., 2005). Ejections of large-scale moving plasma clouds with temperatures probably reaching ~10000 K were detected (Slemzin et al., 2004; Grechnev et al., 2005).

The presented data processing methods were implemented as a software package available at http://www.tesis.lebedev.ru/soft. This package is compatible with SolarSoft (http://sohowww.nascom. nasa.gov/solarsoft/) and is a basis for developing the software of the new space experiment TESIS (Lebedev Physical Institute) onboard the CORONAS-PHOTON satellite. The experiment start is planned for 2008.

ACKNOWLEDGMENTS

The authors are grateful to the instrumental teams of the SOHO and GOES space missions.

This study was supported by the Russian Foundation for Basic Research, project nos. 05-02-17415, 06-02-16106, and 07-02-00101; the Ministry of Education and Science of the Russian Federation (projects NSh-8499.2006.2, NSh-477.2003.2, and NSh-7495.2006.2); program no. 16 of the Physical Science Division of the Russian Academy of Sciences; program of the Presidium of the Russian Academy of Sciences "Solar Activity and Physical Processes in the Sun–Earth System"; and basic research programs of the Physical Science Division of the Russian Academy of Sciences "Plasma Heliophysics" and "Nonstationary Processes in Astronomy".

REFERENCES

1. Kuhn, J.R., Lin, H., and Loranz D. Gain Calibrating Nonuniform Image-Array Data Using Only the Image Data, *PASP*, 1991, vol. 103, p. 1097.
2. Grechnev, V.V., Altyntsev, A.T., Konovalov, S.K., and Lesovoi, S.V., Joint Processing of Radio Data Produced by the SSRT Together with Data of other Spectral Ranges, *Astronomical Data Analysis Software and Systems VIII. ASP Conference Series,* Mehringer, D.M., Plante, R.L., and Roberts, D.A. Eds., 1999, vol. 172, pp. 329–332.
3. Grechnev, V.V., Solar Data Analysis with IDL Software, *Int. Symp. Phys. Processes associated with the Sun*, Weihai, 2002; http://srg.bao.ac.cn/weihailect/Grechnev/Grechnev01.htm.
4. Bugaenko, O.I., Grechnev, V.V., Zhigalkin, R.K., et al., Study of Solar Structures on the Basis of Comprehensive Observations from Ground and the CORONAS-F Satellite: I. Methods of Observations and Analysis of Solar Images Recorded in Various Wave Bands, *Izv. Krymsk. Astrofiz. Obs.*, 2004, vol. 100, pp. 102–114.
5. Slemzin, V.A., Kuzin S.V., Zhitnik I.A., et al., Observations of Solar EUV Radiation with the CORONAS-F/SPIRIT and SOHO/EIT Instruments, *Astron. Vestnik*, 2005, vol. 39, no. 6, pp. 542–549 [Solar System Research (Engl. Transl.) 2005, vol. 39, no. 6, pp. 489–500];
6. Slemzin, V.A., Grechnev, V.V., Zhitnik, I.A., et al., EUV Observations of CME-Associated Eruptive Phenomena with the CORONAS-F/SPIRIT Telescope/Spectroheliograph, *Proc. IAU Symp. 226. "Coronal and Stellar Mass Ejections,"* Dere, K.P., Wang, J., and Yan, Y. Eds., 2005, pp. 21–25;
7. Chertok, I.M. and Grechnev, V.V., Solar Large-Scale Channeled Dimmings Produced by Coronal Mass Ejections, *Astron. Zh.*, 2003, vol. 80, no.2, pp. 162-174 [Astron. Rep. (Engl. Transl.) 2003, vol. 80, no. 2, pp. 139–150].
8. Chertok, I.M. and Grechnev, V.V., Large-Scale Dimmings Produced by Coronal Mass Ejections According to SOHO/EIT Data in Four EUV Lines, *Astron. Zh.*, 2003, vol. 80, no. 11, pp. 1013–1025 [Astron. Rep. (Engl. Transl.) 2003, vol. 80, no. 11, pp. 934–945].
9. Chertok, I.M. and Grechnev, V.V., Large-Scale Activity in the Bastille Day 2000 Solar Event, *Sol. Phys.*, 2005, vol. 229, pp. 95–114; Chertok, I.M. and Grechnev, V.V., Large-Scale Activity in Solar Eruptive Events of October–November 2003 Observed from SOHO/EIT Data, *Astron. Zh.*, 2005, vol. 82, no. 2, pp. 180–192 [Astron. Rep. (Engl. Transl.) 2005, vol. 82, no. 2, pp. 155–166].
10. Chertok, I.M., Slemzin, V.A., Kuzin, S.V., et al., Analysis of a Solar Eruptive Event on November 4, 2001, Using CORONAS-F/SPIRIT Data, *Astron. Zh.*, 2004, vol. 81, no. 5, pp. 447–458 [Astron. Rep. (Engl. Transl.) 2004, vol. 81, no. 5, pp. 407–417].
11. Grechnev, V.V., Chertok, I.M., Slemzin, V.A., et al., CORONAS-F/SPIRIT EUV Observations of October-November 2003 Solar Eruptive Events in Combination with SOHO/EIT Data, *J. Geophys. Res.*, 2005, vol. 110, p. A09S07; doi:10.1029/2004JA010931.
12. Slemzin, V., Chertok, I., Grechnev, V., et al., Multi-Wavelength Observations of CME-Associated Structures on the Sun with the CORONAS-F/SPIRIT EUV

Telescope, *Proc. IAU Symp. 223 "Multi-Wavelength Investigations of Solar Activity,"* Stepanov, A.V., Benevolenskaya, E.E., and Kosovichev, A.G. Eds., 2004, pp. 533–536.

13. Kuzin, S., Chertok, I., Grechnev, V., et al., *CME-Associated Dimmings on the Sun Observed with the EUV SPIRIT Telescope on the CORONAS-F Spacecraft, Adv. Space Res.*, 2006, vol. 38, pp. 451–455.
14. Zarro, D.M., Sterling, A.C., Thompson, B.J., et al., SOHO EIT Observations of Extreme-Ultraviolet "Dimmings" Associated with Halo Coronal Mass Ejections, *Astrophys. J. Lett.*, 1999, vol. 520, pp. L139-L142.
15. Grechnev, V.V., Solar Energetic Particles in SOHO/EIT Images: Cleaning Images and Particle Diagnostics, *Proc. IAU Symp. 223 "Multi-Wavelength Investigations of Solar Activity,"* Stepanov, A.V., Benevolenskaya, E.E., and Kosovichev, A.G. Eds., 2004, pp. 625–626.
16. Grechnev, V.V., A Way to Detect Variable Objects, RF Patent 2 246 760, 2005.
17. Grechnev, V.V., Nakajima, H., and Kundu, M.R., Models and Observations of Impulsive Solar Flares, *Solnechno–Zemnaya Fizika*, 2002, no. 2, pp. 18–20;
18. Grechnev, V.V., A Method to Analyze Imaging Radio Data on Solar Flares, *Sol. Phys.*, 2003, vol. 213, pp. 103–110.
19. Tsiropoula, G., Alissandrakis, C.E., and Mein, P., Association of Chromospheric Sunspot Umbral Oscillations and Running Penumbral Waves I. Morphological Study, *Astron. Astrophys.*, 2000, vol. 355, pp. 375–380.
20. Nindos, A., Alissandrakis, C.E, Gelfreikh, G.V., et al., Spatially Resolved Microwave Oscillations above a Sunspot, *Astron. Astrophys.*, 2002, vol. 386, p. 658–673.
21. Kundu, M.R., Grechnev, V.V., Garaimov, V.I., and White, S.M., Double Loop Configuration of a Flaring Region from Microwave, Extreme-Ultraviolet, and X-Ray Imaging Data, *Astrophys. J.*, 2001, vol. 563, pp. 389–402.
22. Zhitnik, I.A., Kuzin, S.V., Sobelman, I.I., et al., Main Results of the SPIRIT Experiment Onboard the CORONAS-F Satellite, *Astron. Vestnik*, 2005, vol. 39, no. 6, pp. 495–506 [Solar System Research (Engl. Transl.) 2005, vol. 39, no.6, pp. 442–452].
23. Chertok, I.M., Grechnev, V.V., Slemzin, V.A., et al., Manifestation of Coronal Mass Ejections in the EUV Range from the Data of the CORONAS-F/SPIRIT Telescope, *Astron. Vestnik*, 2005, vol. 39, no.6, pp. 517–526 [Solar System Research (Engl. Transl.) 2005, vol. 39, no.6, pp. 462–469].
24. Zhitnik, I.A., Bugaenko, O.I., Ignat'ev, A.P., et al., Dynamic 10 MK Plasma Structures Observed in Monochromatic Full-Sun Images by the SPIRIT Spectroheliograph on the CORONAS-F Mission, *Mon. Notic. Roy. Astron. Soc.*, 2003, vol. 338, pp. 67–71.